Optica Applicata, Vol. XXXIV, No. 1, 2004

Investigation of plasma ablation and crater formation processes in the Prague Asterix Laser System laser facility

STEFAN BORODZIUK[1], ANDRZEJ KASPERCZUK[1], TADEUSZ PISARCZYK[1], SERGEY GUS'KOV[2], JIRI ULLSCHMIED[3], BOZENA KRALIKOVA[4], KAREL ROHLENA[4], JIRI SKALA[4], MILAN KALAL[5], PAWEL PISARCZYK[6]

[1]Institute of Plasma Physics and Laser Microfusion, ul. Hery 23, 00-908 Warszawa 49, Poland

[2]P.N. Lebedev Physical Institute of RAS, 53 Leninski Ave., 119991 Moscow, Russia

[3]Institute of Plasma Physics of the AS CR, Za Slovankou 3, 182 21 Prague 8, Czech Republic

[4]Institute of Physics of the AS CR, Na Slovance 2, 182 21 Prague 8, Czech Republic

[5]Faculty of Nuclear Sciences and Physical Engineering, Czech Technical University in Prague, Brehova 7, 115 19 Prague 1, Czech Republic

[6]Institute of Computer Science, Warsaw University of Technology, ul. Nowowiejska 15/19, 00-665 Warszawa, Poland

The present investigation of the processes of ablative plasma generation and formation of craters was carried out at the Prague Asterix Laser System (PALS) iodine laser facility. Experiments were performed with broad range of laser beam intensities (10^{13}–10^{16} W/cm^2), focal spot radii (35–600 μm), and two laser wavelengths (λ_1 = 1.315 μm and λ_3 = 0.438 μm). The laser beam was focused on the surface of the massive solid aluminum targets. The main goal of our study was to estimate conversion efficiency of the laser beam energy into the energy of shock waves for different mechanisms of laser beam–target interaction. The expansion of plasma generated as a result of the interaction process was observed by means of the 3-frame interferometry. Dimensions and shapes of the craters were determined using optical microscopy and wax-replica technique.

Keywords: laser-produced plasma, interferometric measurements, crater, laser beam intensity distribution, absorption mechanism.

1. Introduction

In this paper, results of experimental studies aimed at detailed investigation of powerful laser pulses interacting with massive solid targets are presented. Experiments were performed with broad range of laser beam intensities (10^{13}–10^{16} W/cm^2), focal spot radii (35–600 μm), and two laser wavelengths (λ_1 = 1.315 μm and λ_3 =0.438 μm). The laser pulse duration of ~0.4 ns was kept constant in all shots.

This set-up allowed for $I\lambda^2$ parameter to be varied over the four orders of magnitude (2×10^{12}–2×10^{16} Wμm^2/cm^2) thus making it possible not only to perform the essential interaction studies but also to look for experimental verification of theoretical predictions concerning the processes under consideration [1], [2].

First of all, the lower $I\lambda^2$ range of 2×10^{12}–10^{14} Wμm^2/cm^2 corresponds to a full domination of the classical inverse bremsstrahlung absorption mechanism of laser radiation, while in the case of $I\lambda^2 > 10^{15}$ the resonance absorption mechanism plays the dominant role with the fast electrons responsible for the absorbed laser energy transfer into the solid part of the target.

The use of subnanosecond laser pulses allowed the testing of the shock wave generation due to ablative pressure short duration reaction time in comparison with the characteristic time of the shock wave damping within the solid target as well as the crater creation period, thus making it possible to separate the processes of plasma corona creation and shock wave propagation inside the non-evaporated part of the target. Moreover, variation of the focal spot radius on the target surface made it possible to investigate an influence of intensity distributions of the laser beam on plasma corona features and crater parameters.

The problems analysed in this paper are typical not only in investigation of the fundamental processes taking place during the laser beam–matter interaction, *i.e.*, absorption of laser radiation within created plasma, evaporation of target material, shock wave generation in non-evaporated part of the target, *etc.*, but for practical applications connected with technology of material working and inertial thermonuclear fusion.

2. Experimental set-up

The experiment was carried out with the use of the PALS iodine laser facility [3]. The laser system, together with a 3-frame interferometric set-up, is shown schematically in Fig. 1. It consists of a generator and five amplifiers. All amplifiers need to be switched on when the output laser energy of the order of 300 J and above is required.

Plasma was generated by the laser beam with its diameter at the target chamber about 290 mm focused by means of an aspherical lens on the surface of a planar solid target made of aluminum. As part of the study, two harmonics of the laser radiation (the first one with a wavelength of $\lambda_1 = 1.315$ μm and the third one with $\lambda_3 = 0.438$ μm) were used. The third harmonic was generated in a DKDP crystal. The conversion efficiency is shown in Fig. 2. It is necessary to point out that the output laser energy is not equal to the energy of the laser beam on the target due to energy losses along the path to the experimental chamber. These losses are around 33%. The laser energy, denoted by E_L, corresponds to the real energy on the target. The essential part of the investigation was carried out with the laser energy $E_L \cong 100$ J. Some shots for λ_1 were also carried out with $E_L \cong 600$ J.

The range of different intensities of the laser radiation on the target was obtained mainly by changing the focal lens position. The maximum intensity achieved on the

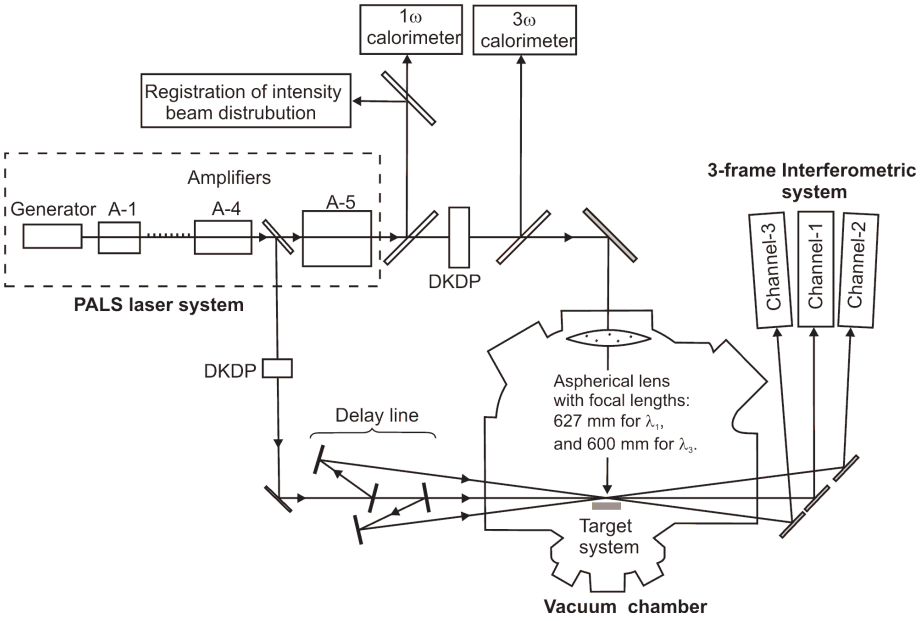

Fig. 1. Experimental set-up.

target corresponded to the minimum focal spot radius of 35 μm. The investigation was carried out for the focal spot radii R_L = 35, 100, 300 and 600 μm.

Intensity distributions in the laser beam cross-section were recorded by the CCD camera. This allowed us to observe some irregularities in the intensity distributions connected with the output laser energy. Namely, to obtain the output laser energy below

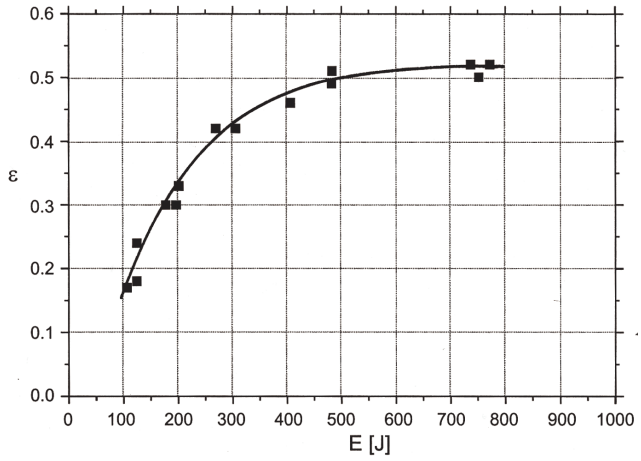

Fig. 2. Efficiency of the laser wavelength conversion of the first and the third harmonic of the iodine laser beam.

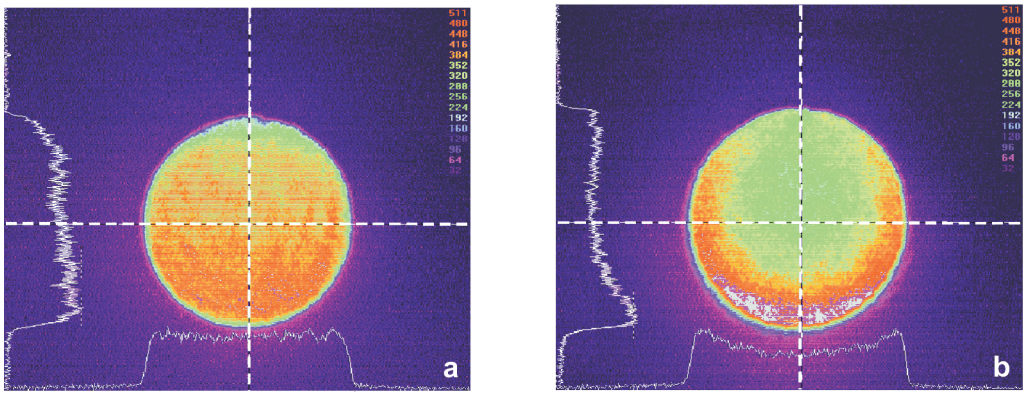

Fig. 3. Intensity distributions in the cross-section of the laser beam for the first harmonic of the heating beam in the cases of E_L = 100 J (**a**) and E_L = 600 J (**b**).

180 J, the last amplifier had to be switched off. In this case the intensity distribution had approximately a flat character along the radius (see Fig. 3**a**). For higher energies, when all the amplifiers worked, the intensity distribution became concave (Fig. 3**b**). This feature is due to amplifying characteristics of the iodine laser amplifiers which amplify more in the off-axis region. After passing through the first four amplifies the generated laser beam changes its shape from the Gaussian-like distribution into the flat one. The last amplifier additionally makes the cavity in the center of this distribution, the depth of which increases with increasing laser energy. This concave character of the intensity distribution is even more pronounced in the case of the third harmonic due to the nonlinear conversion of the DKDP crystal. This detail knowledge becomes essential in understanding certain specific features of experimental results.

To study the expansion of the ablative plasma a 3-frame interferometric system with automated image processing [4] was employed. The diagnostic system was illuminated by the third harmonic of the iodine laser. The delay between subsequent frames was set to 3 ns. In this arrangement the interferometric measurement during a single shot covered a period of 6 ns only. In order to probe later stages of the plasma expansion, the initial time of the observation was delayed in some shots by additional 6 ns. High reproducibility of the plasma expansion at different laser shots with the same parameters made it possible to sew interferogram sequences from different shots together. Owing to this, our observation period could be extended up to 12 ns, starting from 3 ns after the maximum of the heating laser pulse.

3. Analysis of the experimental results

3.1. Dimensions and shape of craters

The crater dimensions, *i.e.* crater radius R_c and crater depth H_c, were measured by means of optical microscopy measurements. In order to determine the exact shapes of the craters, crater replicas were made of wax.

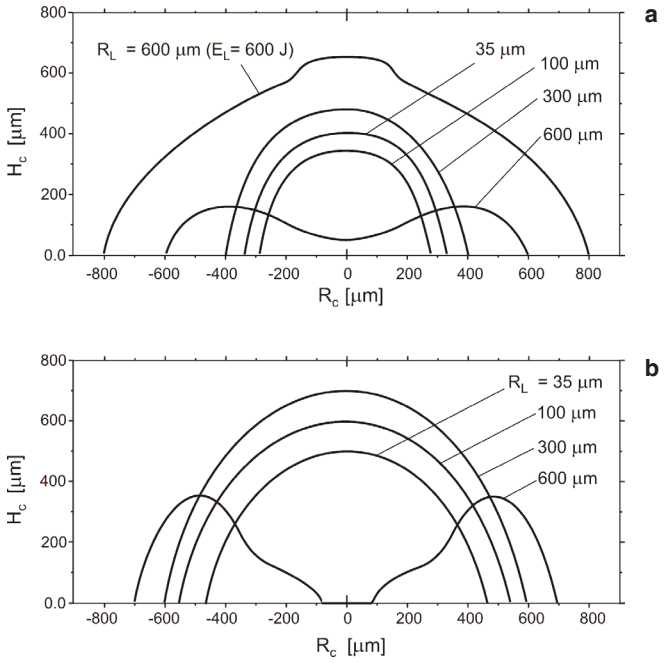

Fig. 4. Crater shapes and dimensions for the first (**a**) and the third (**b**) harmonics of the heating beam.

The results of these measurements for both harmonics at E_L = 100 J of the laser energy are presented in Fig. 4. Additionally, in Fig. 4**a**, an example of the crater for E_L = 600 J is also shown.

In the experiment with E_L = 100 J, excluding the cases for R_L = 600 μm, all craters assumed approximately a hemispherical shape. For R_L = 600 μm the craters have the shape close to a hemitorus. The craters produced by laser pulses with shorter wavelength (λ_3) are visibly larger (3–4 times) than those produced by the longer one (λ_1). The hemitoroidal shapes for both wavelengths clearly differ form each other, too. Moreover, for wavelength λ_3 the non-evaporated part of the target in the central region is observed. This fact is easy to understand taking into account the intensity distribution of the iodine laser beam discussed earlier. The form closer to the hemitoroid in the case of wavelength λ_3 corresponds to the more pronounced concave $I(r)$ distribution. Taking into account the efficiency of the wavelength conversion in DKDP crystal (see Fig. 2) and the losses of the output laser energy mentioned earlier, to achieve the final energy on the target of around 100 J, the output laser energy above 300 J is needed. This means that all the amplifiers are switched on and the laser beam cross-section assumes the concave form of $I(r)$.

The hemispherical form of the craters in the case of the remaining focal spot radii is connected with relatively strong irradiation of small areas on the target. The shock waves generated in these conditions are strong enough to reach the axis and to assume the hemispherical form. A similar situation is observed in the case of R_L = 600 μm

for E_L = 600 J (see Fig. 4**a**). Here, the shock wave (stronger in comparison to that for 100 J) also reaches the axis and the crater shape is no longer hemitoroidal.

In Figure 5, the dependences of the crater volume V_{cr}, and I, $I\lambda_1^2$, $I\lambda_3^2$ as a function of the focal spot radius for both wavelengths are shown. For our qualitative analysis it was assumed that the focal spot is uniformly irradiated. On the basis of this figure some interesting features of the crater creation can be observed.

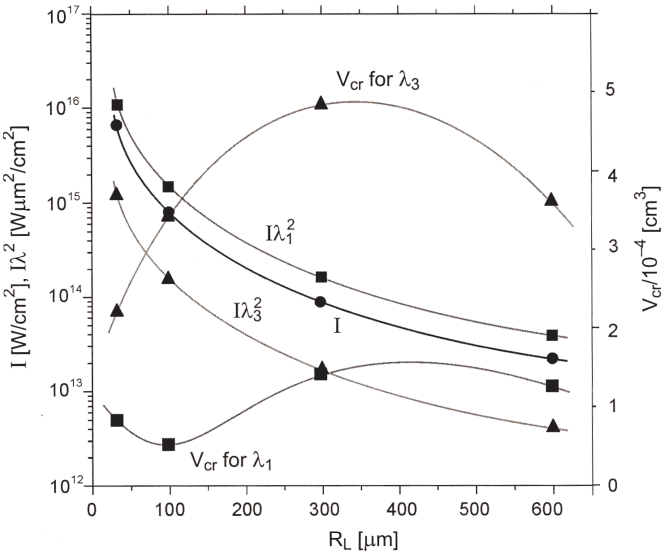

Fig. 5. Diagrams of the crater volumes for λ_1 = 1.315 μm and λ_3 = 0.438 μm as well as diagrams of I, $I\lambda_1^2$, and $I\lambda_3^2$ *vs.* time.

The dependence of $V_{cr}(R_L)$ for λ_3 becomes parabolic with the clear maximum around R_L = 300 μm. In the case of λ_1, the crater volume dependence is more complex. The curve of $V_{cr}(R_L)$ for R_L > 100 μm assumes a form similar to that for λ_3 but the maximum of this function is less pronounced. For R_L < 100 μm, however, instead of a decrease of V_{cr} with decreasing R_L an increase of V_{cr} is observed. It is obvious that the crater volume, *i.e.*, amount of the ejected target material, depends on the efficiency of the laser–target interaction. In terms of a qualitative analysis of the above difference one can come to a conclusion that this effect is connected with a change of the governing mechanism of the laser beam–target interaction for $I > 10^{15}$ W/cm^2 during the transition from λ_1 to λ_3. Taking into account that for R_L = 35 μm the parameter $I\lambda_1^2 = 1.2\times10^{16}$ Wμm^2/cm^2 is by an order of magnitude larger than $I\lambda_3^2 = 1.3\times10^{15}$ Wμm^2/cm^2 one can come to the conclusion that in the case of λ_1 the resonance absorption plays the dominant role unlike in the case of λ_3, where absorption is realized by the inverse bremsstrahlung.

The investigation of the dimensions of craters allows us to draw the following essential conclusions:

– for a given energy and duration of the laser pulse the crater size, becoming an indicator of the efficiency of the laser energy transferred into a shock wave, strongly increases with a decrease of the wavelength of the laser radiation in a broad range of radiation intensities, *i.e.*, from 2×10^{13} to 7×10^{15} W/cm^2;

– in the case of the first harmonic, the transition through the intensity of 10^{15} W/cm^2 is connected with a change of the character of the laser beam–plasma interaction, *i.e.*, the inverse bremsstrahlung absorption for lower intensities is replaced by the resonance absorption.

3.2. Results of the interferometric measurement

Complementary information about the plasma creation and crater formation processes was obtained from interferometric measurements. On the basis of registered interferograms it was possible to reconstruct the free electron density distributions at different instants of plasma stream expansion. Some results of interferometric measurements and computer calculation are presented in this chapter. For this calculation the numerical methods, described in paper [5], were used.

In Figure 6, sequences of electron density distributions for both wavelengths correspond to the two particular cases: the minimum radius of the focal spot (R_L = 35 μm) and the radius of 300 μm (optimum from the point of view of the crater creation). The electron density distributions are presented in the form of isodensitograms. Analogous sequences of the electron density isodensitograms for R_L = 600 μm, but with the frames temporal separation twice as large (6 ns), are shown in Fig. 7. The plasma stream boundary is represented here by the electron density contour $n_e = 2\times10^{17}$ cm^{-3}. The second equidense corresponds to $n_e = 3\times10^{18}$ cm^{-3} and all subsequent equidensity lines are always separated by $n_e = 3\times10^{18}$ cm^{-3}.

Figure 8 contains diagrams of the total free electron number N_e for E_L = 100 J as a function of the time for both wavelengths and all the focal spot radii.

At the beginning of the analysis of the interferometric measurement results let us make use of the total free electron number. In the case of approximation of the average plasma charge Z, the mass of the plasma stream M_p corresponding to N_e is expressed by the formula:

$$M_p = N_e\, m_p \frac{A}{Z}$$

where: m_p – proton mass, and A – atomic weight of plasma ions.

According to the above equation, a very rough estimation of the plasma stream mass at the instant of 3 ns for all the cases under consideration gives values which fall within the range of 10^{-7}–10^{-6} g. For a real ionization degree the range of the mass

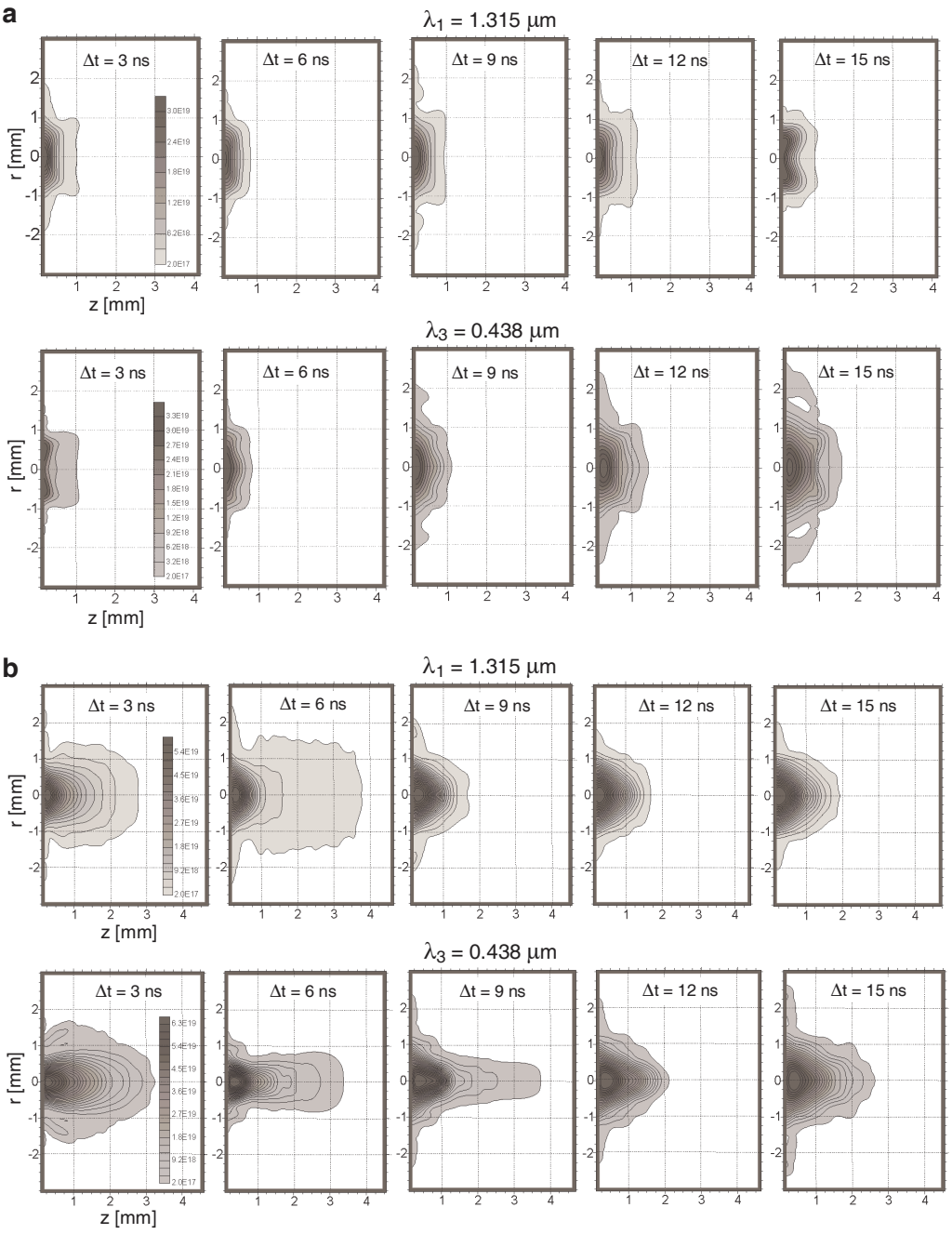

Fig. 6. Sequences of the electron density isodensitograms for the two particular cases: R_L = 35 μm (**a**) and R_L = 300 μm (**b**).

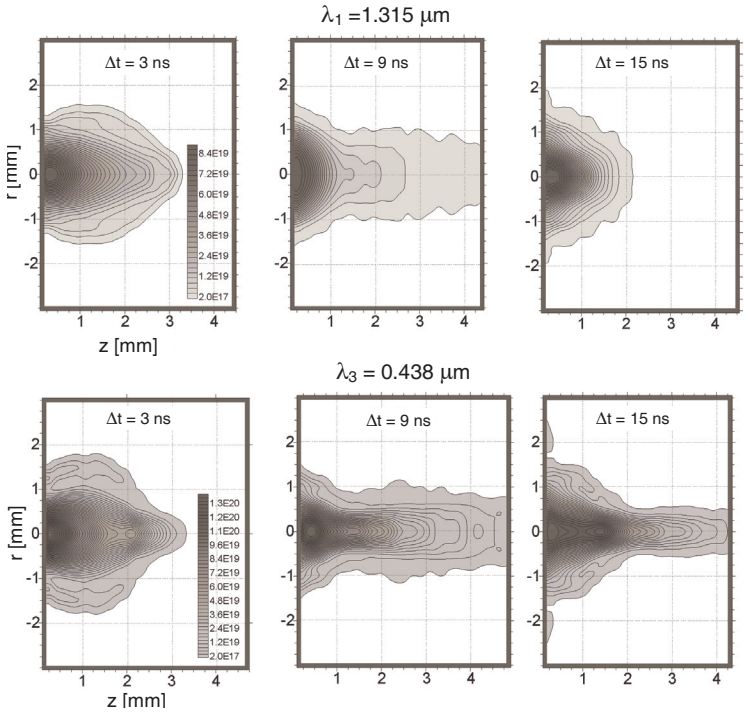

Fig. 7. Sequences of the electron density isodensitograms for R_L = 600 μm.

values could be increased by the factor 2–3. In the period of the interferometric measurement (3–15 ns) the plasma stream mass changes, but its value remains in the range mentioned above. From the wax replicas it was found that the crater masses are in the range of 10^{-4}–10^{-3} g. The apparent difference between the masses of the plasma streams and that of craters shows that the interferometric investigation deals mainly with the ablative plasma evaporated during the laser beam action. This conclusion can be additionally confirmed by a very small difference between the plasma stream masses for the first and the third harmonics, especially for the first two instants of the measurements, *i.e.*, for 3 and 6 ns, while the crater masses for λ_3 are 3–4 times larger in comparison with that for λ_1.

During the plasma stream formation, a few physical processes take place, such as hydrodynamic processes, ionization, recombination and the like. Thus an unambiguous explanation of the temporal evolution of the total electron number is rather difficult. Nevertheless, the overall tendency of the N_e to increase with time, especially in relatively late times of $t > 9$ ns, could likely be caused by contribution of the plasma outflow created by the shock wave during the initial stage of its propagation.

Let us consider the analysis of the electron density distribution of the plasma stream. First of all, attention should be paid to qualitative features of the data presented.

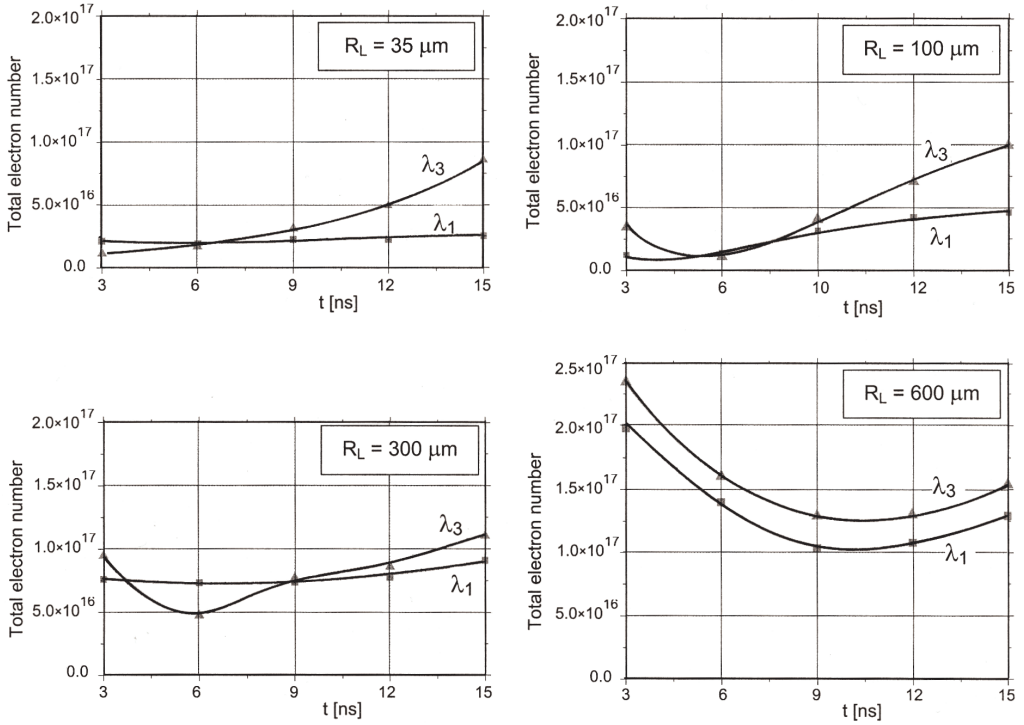

Fig. 8. Diagrams of the temporal changes of the total free electron number for different radii of the focal spot.

The temporal evolution of any particular equidense position can provide only qualitative information about the plasma expansion velocity. It is connected with the change of the electron density during the plasma expansion due to the recombination process. Even when the degree of ionization is conserved, temporal evolution of any equidense corresponds to its motion with a phase velocity since plasma can leak through the surface denoted by this equidense. Nevertheless, the considerably larger dimensions of the plasma stream for R_L = 300 μm in comparison with that for R_L = 35 μm (especially in the axial direction) in the same instants of time (see Fig. 6) can only mean the velocity increase by the factor of 1.5–2 in the first case.

Secondly, the flat shape of equidensity lines in front of the expanding plasma in the case of R_L = 35 μm (Fig. 6**a**) testifies to the relatively homogeneous distribution of beam intensity. Contrary to that, in the cases of greater R_L the shape of the equidensity lines corresponds to the non-homogeneous distribution of the beam intensity with the maximum located in the peripheral region of the beam cross-section. Actually, the shape of the equidenses of the dense component of the plasma stream for R_L = 300 μm at 3 and 6 ns (Fig. 6**b**) and, especially for R_L = 600 μm at 3 ns (Fig. 7) suggests that the plasma stream expands in the space between the two co-axial conical

surfaces. The inner cone is convergent to the axis, the outer one is, on the contrary, divergent. Moreover, the shape of equidenses at the later times clearly demonstrates cumulative impact on the axis of the inner component of the plasma stream. These processes result in a considerable elongation of the plasma stream along the axis. The plasma stream elongation and the appearance of such dense plasma so far from the target surface are not only connected with an increase of the plasma stream mass due to concentration of the plasma on the axis, but also with a secondary plasma ionization due to an increase of plasma temperature during the process of the cumulative impact of the plasma stream.

Finally, let us focus our attention to Fig. 8**d**, where the dependence of the total free electron number on the time for R_L = 600 μm is presented. The diagrams show that after an initial phase of the N_e decrease as a result of plasma recombination, at the moment of about 9 ns a strong growth of N_e is observed. At this moment the cumulative impact of the plasma stream occurs (see Fig. 7). This correlation confirms the appearance of the secondary ionization of plasma which leads to the growth of the total electron number.

4. Conclusions

PALS facility provided the opportunity to employ extreme parameters of the laser beam for experimentation. The available broad ranges of I and $I\lambda_2$ made it possible to investigate different laser radiation absorption mechanisms in the processes of both the plasma creation and the shock wave generation. The key role in these studies was fulfilled by the interferometric diagnostic which delivered a considerable amount of interesting information thanks to the possibility of the plasma stream vizualization and determination of the electron density distribution.

Most importantly, the interferometric measurements clearly demonstrated that the expansion of the ablative plasma lasts up to 9–12 ns after the action of the laser pulse. During the final stage of the ablative plasma outflow, slight participation of the plasma stream generated by the shock wave was also observed.

Both the crater investigation and the interferometric measurements revealed the direct connection between the laser beam intensity distribution and the processes of plasma generation and crater creation. It was discovered that certain features of the iodine laser beam allowed the cumulative plasma stream creation. This effect could be used for investigation of fundamental processes which occur in the hot and dense plasma. Moreover, the elongated plasma stream could be considered as a potentially suitable configuration for propagation and amplification of the coherent radiation of the X-ray laser.

Acknowledgements – This work was partially supported by the European Committee program Transnational Access to Research Infrastructures under contract HPRI-CT-1999-0053 (PALS project 013), the Russian Foundation of Basic Research (Project # 02-02-16966), IAEA (Research Project No. 11655/RBF).

References

[1] GUS'KOV S.YU., ZVEREW V.V., ROZANOV V.B., Quantum Electron. **13** (1983), 498.
[2] GUS'KOV K.S., GUS'KOV S.YU., Quantum Electron. **31** (2001), 305.
[3] JUNGWIRTH K., CEJNAROWA A., JUHA L., KRALIKOVA B., KRASA J., KROUSKY E., KRUPICKOVA P., LASKA L., MASEK K., MOCEK T., PFEIFER M., PRAG A., RENNER O., ROHLENA K., RUS B., SKALA J., STRAKA P., ULLSCHMIED J., Phys. Plasmas **8** (2001), 2495.
[4] KALAL M., GUS'KOV S., GROMOV A.I., KASPERCZUK. A., KONDRASHOV V.N., KROUSKY E., KRALIKOVA B., LIMPOUCH J., MASEK K., PISARCZYK T., PFEIFER M., ROHLENA K., ROZANOV V., SKALA J., STRAKA P., ULLSCHMIED J., Fusion Sci. Technol. **43** (2003), 275.
[5] KASPERCZUK A., PISARCZYK T., Opt. Appl. **31** (2001), 571.

Received November 11, 2003